Nanoscale

ARTICLE

Citrate-stabilized Gold Nanoparticles hinder fibrillogenesis of a pathologic variant of β_2-microglobulin

Received 00th January 20xx,
Accepted 00th January 20xx

DOI: 10.1039/x0xx00000x

www.rsc.org/

Cristina Cantarutti,[a] Sara Raimondi,[b,c] Giorgia Brancolini, [d] Alessandra Corazza,[a,c] Sofia Giorgetti,[b,c] Maurizio Ballico,[e] Stefano Zanini,[e] Giovanni Palmisano,[f] Paolo Bertoncin,[g] Loredana Marchese,[b,c] P. Patrizia Mangione,[b,c,h] Vittorio Bellotti,[b,c,h] Stefano Corni,[d] Federico Fogolari,[a,c] and Gennaro Esposito [a,c,e]

Nanoparticles have repeatedly been shown to enhance fibril formation when assayed with amyloidogenic proteins. Recently however evidence casting some doubt about the generality of this conclusion started emerging. Therefore, to investigate furtherly the influence of nanoparticles on the fibrillation process, we used a naturally occurring variant of the paradigmatic amyloidogenic protein β_2-microglobulin (β2m), namely D76N β2m where asparagine replaces aspartate at position 76. This variant is responsible for an aggressive systemic amyloidosis. After characterizing the interaction of the variant with citrate-stabilized gold nanoparticles (Cit-AuNPs) by NMR and modeling, we analyzed the fibril formation by three different methods: thioflavin T fluorescence, native agarose gel electrophoresis and transmission electron microscopy. The NMR evidence indicated a fast-exchange interaction involving preferentially specific regions of the protein that proved, by subsequent modeling, to be consistent with a dimeric adduct interacting with Cit-AuNPs. The fibril detection assays showed that AuNPs are able to hamper D76N β2m fibrillogenesis through an effective interaction that competes with protofibril formation or recruitment. These findings open promising perspectives for the optimization of nanoparticle surface to design tunable interactions with proteins.

Introduction

The impact of nanotechnologies in biomedicine, biophysics and biotechnology is becoming extremely challenging for the number of issues that are raised and the specific research demands thereof not only for applicative technology but also for basic research.[1,2] In particular, the interaction of nanoparticles (NP), and specifically the very versatile gold nanoparticles (AuNPs), with proteins is crucial for any application in drug delivery, imaging, diagnostics, etc.[3] It is widely accepted that the surface of nanoparticles adsorbs proteins either transiently or permanently in the so-called soft or hard corona layer, respectively.[1] As a consequence, the protein structure and/or function may be changed to different extent or likewise remain conserved. We have recently addressed the interaction of citrate-capped gold nanoparticles (Cit-AuNPs) with β2-microglobulin (β2m),[4] the light chain component of class I major histocompatibility complex (MHCI) that in long-term hemodialyzed patients precipitates into amyloid deposits and accumulates in the collagen-rich tissues of the joints, originating a pathology referred to as dialysis related amyloidosis (DRA).[5] Besides the pathological relevance, β2m has proven a very convenient system for in vitro and in vivo studies as it recapitulates several paradigmatic aspects of the amyloid transition. Based on molecular dynamics and electrostatics calculations confirmed by experimental NMR evidence,[4] we showed that under neutral conditions β2m preserves its structure in the presence of Cit-AuNPs, without undergoing any amorphous aggregation and precipitation or fibrillar transition. A preferential interaction between the protein and the stabilized nanoparticles could be mapped both theoretically and experimentally, with an observed regime featuring the soft-corona-like interaction dynamics. These findings can be regarded as a proof of concept for designing

[a] DSMB, Università di Udine, P.le Kolbe 4, 33100 Udine, Italy,
[b] Dipartimento Medicina Molecolare, Università di Pavia, Via Taramelli 3, 27100 Pavia, Italy,
[c] INBB, Viale Medaglie d'Oro 305, 00136 Roma, Italy,
[d] CNR Istituto Nanoscienze, Via Campi 213/A, 41125 Modena, Italy,
[e] Science and Math Division, New York University at Abu Dhabi, Abu Dhabi, UAE,
[f] Department of Chemical and Environmental Engineering, Masdar Institute of Science and Technology, PO Box 54224, Abu Dhabi, UAE,
[g] Dipartimento Scienze della Vita, Università di Trieste, Via Weiss 2 , 34128 Trieste, Italy,
[h] Division of Medicine, University College of London, London NW3 2PF, UK.

† Electronic Supplementary Information (ESI) available: bar plots of all available NMR cross-peak attenuations, relevant collective motions of the protein dimer components from principal component analysis and three native agarose gel electrophoresis that were obtained under different experimental conditions. See DOI: 10.1039/x0xx00000x

systems and establishing conditions to set up observations of amyloidogenic proteins and nanoparticles, without necessarily increasing rate and extent of fibrillar transformation as observed in earlier investigations.[6] The results were exploited to progress further in monitoring nanoparticle effects by challenging a species that could undergo fibrillogenesis under mild conditions at neutral pH. We used therefore D76N β2m, a naturally occurring variant of β2m bearing an asparagine residue at position 76 instead of an aspartate, that is responsible for a severe systemic amyloidosis.[7] This variant readily forms fibrils by agitation at neutral pH exhibiting the highest amyloidogenic ability amongst all known β2m variants.[7] We found that Cit-AuNPs indeed affect fibrillogenesis of D76N β2m and here we describe the characteristics of the interaction that once again confirms the interesting and advantageous properties of AuNP-based systems.

Results and discussion

Preliminary assessment of protein-NP preparations

The synthesized (see Experimental section) citrate-stabilized Au nanoparticles preparations without and with protein, were preliminarily controlled by UV-Vis spectroscopy and transmission electron microscopy (TEM). The colloidal nature of the solution was confirmed by the presence of the Surface Plasmon Band[9,10] (SPB) in the UV-Vis spectrum, with a maximum at 518 nm compatible with Cit-AuNPs dimensions in the wanted range (5-10 nm) that shifted as expected[12] upon protein addition (Fig. 1). Analysis of the images obtained by TEM gave an average diameter of 7.5 ± 1 nm for the prepared Cit-AuNPs (Fig. 2a). No size change was observed in the presence of D76N β2m, ruling out any NP aggregation onset (Fig. 2b).

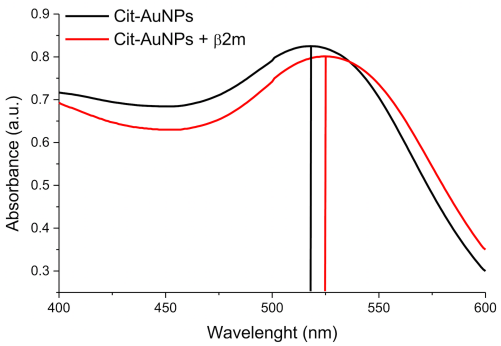

Fig. 1 Absorption spectra of Cit-AuNPs alone (black line) and of Cit-AuNPs with 20 μM D76N β2m (red line). The black and red vertical lines show the position of the absorbance maximum of the solution in absence and in presence of the protein, respectively. The SPR band shifts from 518 nm to 525 nm upon addition of the protein.

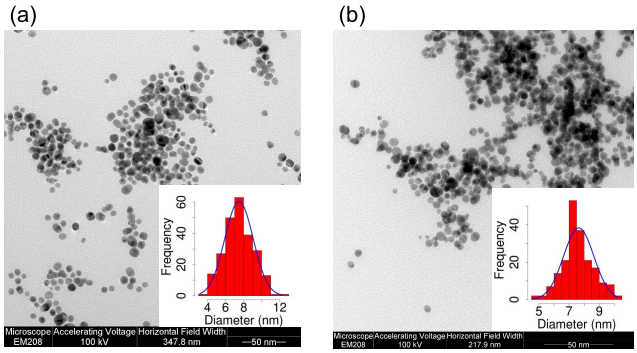

Fig. 2 TEM micrographs of synthesized Cit-AuNPs (a) alone and (b) incubated with 20 μM D76N β2m, along with the corresponding size histograms shown in the insets. The size distribution in presence of D76N β2m rules out a possible protein-induced aggregation.

Binding of wild-type and D76N β2m to Cit-AuNPs

The AuNPs capability to quench tryptophan (Trp) fluorescence is a very convenient effect that can be exploited to investigate their interaction with proteins bearing fluorescent Trp residues, in terms of binding affinity and Trp accessibility.[13] β2m intrinsic fluorescence is mainly due to a buried Trp residue, namely Trp95. The second Trp residue of the molecule, Trp60, contributes only marginally to the overall fluorescence because of its exposure on the protein surface and the consequent quenching effect of the solvent (Fig. 3).[14] In presence of Cit-AuNPs, the shape and the position of β2m emission spectra is preserved (Fig. 4), meaning that the protein conserves the native folding in agreement with the NMR and MD evidences reported previously[4] and in the next sections.

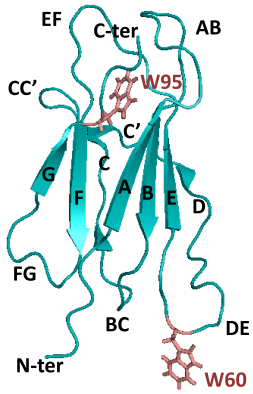

Fig. 3 Cartoon of β2m structure showing the positions of Trp60 (W60) and Trp95 (W95) depicted in salmon pink. The β2m strand and loop naming is also indicated.

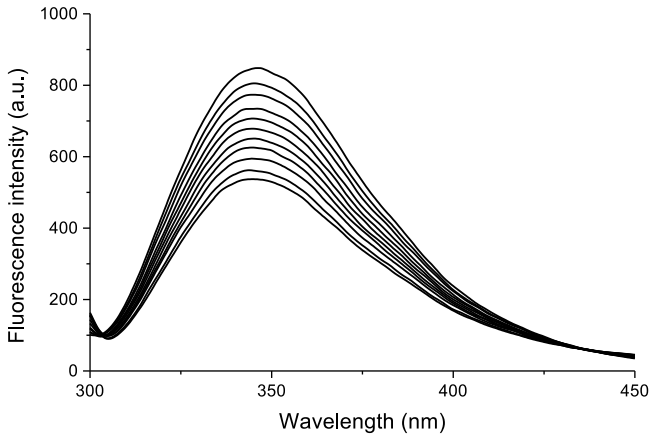

Fig. 4 Fluorescence quenching of 0.5 μM wild-type β2m with Cit-AuNPs concentrations ranging from 0 nM to 0.8 nM.

The decrease of protein fluorescence intensity shows a linear trend as a function of nanoparticle concentration (Fig. 5a), since the amount of interacting quenched protein increases proportionally with the available concentration of binding sites on the nanoparticle surface.

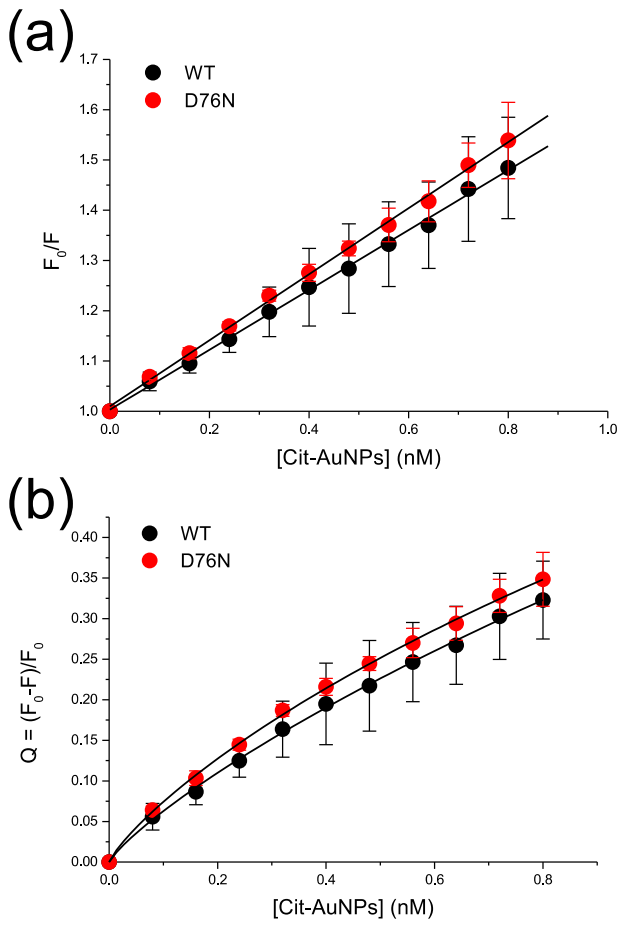

Fig. 5 Wild-type (WT) and D76N β2m fluorescence quenching data fitted by (a) the Stern-Volmer equation[15] and (b) the Hill equation.[16] Data are presented as average of three independent experiments and the error is the standard deviation.

The same behaviour was observed for the wild-type and for the tested amyloidogenic variant (Fig. 5). The efficacy of the quenching in spite of the very low concentration of Cit-AuNPs (the quencher) would suggest that the most appropriate interpretation of the interaction process is a dynamic model that entails a non-equilibrium transient interaction between the protein and the quencher.[16] As a check, we applied the Hill equation[16,17] to the fluorescence data (Fig. 5b) to estimate the apparent dissociation constants (K_d).

The values obtained from the fitting are reported in Table 1 and indicate that indeed we deal with a transient interaction regime that consistently does not exhibit any cooperativity (that would entail a Hill coefficient, *n*, larger than unity). The dissociation constants in fact are in the range of 10^{-9} M, i.e. the reciprocal of the K_{SV} slope of the Stern-Volmer plot in Fig. 5a. A static model with $K_d = 10^{-9}$ M is inconsistent with the NMR experimental evidence (we observed[4] protein signal attenuations well beyond the expected saturation level that should be quickly reached if the K_d is in the nM range). However the dynamic nature of the process can not be purely collisional because within this picture, and taking into account that tryptophan fluorescence lifetimes (τ_0) in proteins range between 1 and 10 ns,[17] the bimolecular quenching constant (k_q) would be 10^{17}-10^{18} M^{-1} s^{-1}, which is unphysical. The dynamic quenching must arise from other mechanisms, i.e. RET (Resonant Energy Transfer) or photoinduced electron transfer.[17,18] Since the variant W60G β2m, bearing a single tryptophan residue at position 95, exhibits the same fluorescence quenching pattern as observed with wild-type and D76N β2m species (data not shown), an intramolecular donor-acceptor transfer mechanism, i.e. FRET (Förster Resonant Energy Transfer), can be safely ruled out. Both protein tested gave K_{SV} values in the same range without a statistically significant difference. This means that the extent of interaction with Cit-AuNPs is about the same for wild-type β2m as for the amyloidogenic variant. These results, along with previous findings,[4] suggest that there is a fast and efficient interaction between β2m and Cit-AuNPs that does not affect the protein structure. Moreover, these conclusions can be extended to the naturally occurring amyloidogenic variant D76N β2m.

Mapping the interaction of D76N β2m with Cit-AuNPs

Three pairs of D76N β2m solutions were prepared with concentrations ranging between 4.5 and 18 μM, with and without Cit-AuNPs (always 84 nM). The corresponding protein/NP ratios ranged between 53 and 213.

Table 1 Parameters obtained from fluorescence quenching data fitted with Hill equation for wild-type and D76N β2m. See Experimental section for error calculation.

Protein	Wild-type β2m	D76N β2m
K_a /10^9 M^{-1}	2.00 ± 0.08	1.92 ± 0.055
Hill coefficient	0.954 ± 0.028	0.906 ± 0.020
R^2	0.996	0.999

Commercially available nanoparticles with average diameter of 5 nm were used for the NMR analysis to better compare the measurements with D76N β2m to the precedent results with wild-type species.[4] ^{15}N-^{1}H HSQC spectra were collected and the nitrogen-hydrogen correlations, predominantly arising from the backbone amides, were comparatively sampled to assess the effect of Cit-AuNPs on frequencies and amplitudes. Exactly as observed with wild-type β2m,[4] we found no chemical shift variation at any of the chosen protein/NP ratios. We observed, instead, intensity changes, that appeared unevenly distributed over the protein signals. The results were repeatedly confirmed over several months on the same samples. Fig. 6a depicts the 2D map overlay of the spectra obtained at the intermediate D76N β2m concentration and ratio relative to Cit-AuNPs (protein/NP = 107). The projections on top of the map more clearly show the attenuation the protein signals undergo in the presence of nanoparticles. The average intensity ratio between the corresponding peaks of the spectra overlaid in Fig. 6a is 0.61 with a standard deviation over all the sampled peaks of ±0.04 (essentially equal to the average volume ratio of the same data). Similar attenuations were obtained also for the other explored conditions (0.73±0.07and 0.78±0.04, at protein/NP ratio of 53 and 213, respectively). In fact, based on the signal-to-noise ratio of the 2D maps, the uncertainties of the average attenuations can be estimated to be 16%, 8.5% and 2.7%, respectively, as the protein/NP ratio increases, which reduces the significance of

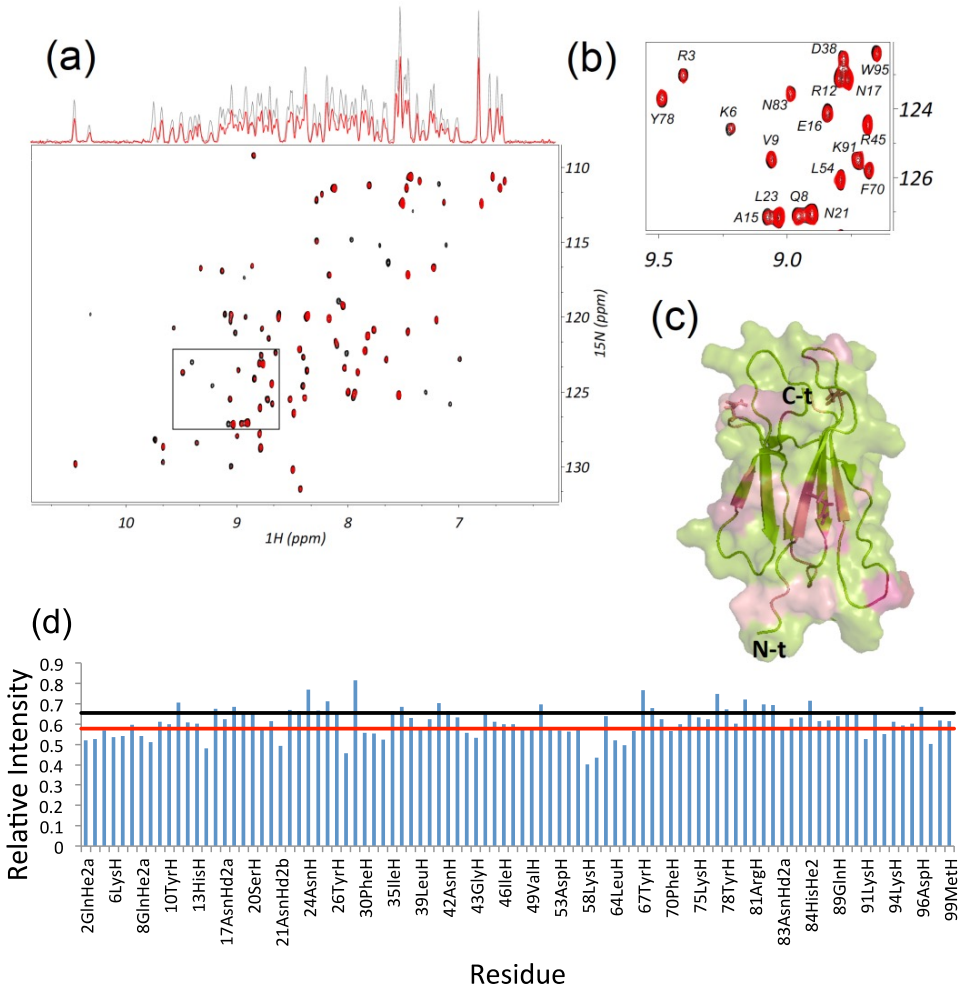

Fig. 6 (a) Superimposition of corresponding ^{15}N-^{1}H HSQC regions obtained from 8.9 μM D76N β2m samples without (black) and with (red) Cit-AuNPs (84 nM, protein/NP ratio of 107). The relative positive peak projections are reported on top of the contour map overlay to highlight the NP-induced attenuation. The contour maps and the projections are drawn on the same absolute scale. The rectangular insert is expanded in (b) where the drawing scale for the red contours (sample with Cit-AuNPs) is increased by 50%. The corresponding backbone amide assignments are reported by single letter code. (c) D76N β2m cartoon highlighting the residue locations that proved most affected by Cit-AuNPs. i.e. displaced one standard deviation at least with respect to the average attenuation. For residues exhibiting attenuations at the side-chain rather than backbone amide (Gln8, Asn21, Asn42), a side-chain stick representation is reported. Refer to Fig. 3 scheme for strand and loop naming. N-t and C-t stand for N-terminus and C-terminus, respectively. (d) Bar plot of individual peak attenuations calculated as intensity ratios of the corresponding

signals in the spectra overlaid in (a). The two horizontal lines indicate the standard deviation levels above and below the average attenuation.

their differences, especially for the lowest concentration condition. These features suggest that the interaction between D76N β2m and Cit-AuNPs propagates quite efficiently under the considered experimental conditions, featuring the same fast interaction regime as observed for wild-type β2m.[4] The analogy with respect to the previously reported results extends further. The intensity ratio profile reported in the bar plot of Fig. 6d shows that there were regions of D76N β2m exhibiting increased attenuation. As for the earlier study,[4] we can attribute this to preferential interaction with Cit-AuNPs. It should be recognized, however, that a change in signal intensity (and/or frequency) may also reflect the consequence of an allosteric perturbation related to the interaction, if the molecular size, mobility and interaction regimes are suitable. Typically these allosteric effects are easily recognised when buried regions undergo rearrangements in response to processes involving the molecular surface. Attenuations beyond a single standard deviation from the average are seen in Fig. 6d at the locations listed in Table 2. Essentially the same pattern was confirmed at the other explored protein/NP ratios (ESI Fig. S1†). The attenuation of some side-chain carboxyamides might reflect effects from solvent exchange or possible solvent occupancy differences instead of direct interaction with Cit-AuNPs, since the extent of side-chain signals appears often affected by the efficiency of the selective flip-back pulse used in the HSQC sequence to suppress the solvent magnetization.[19]

Table 2 NMR attenuations of D76N β2m backbone and side-chain amides vs. interface residues of D76N β2m dimer from MD-refined docking.

Structure region	NMR attenuations	Simulated dimer interface
N-term, A strand	2sc, 3, 6, 7, 8sc	4, 5
AB loop	13, 16	
B strand	21sc, 28	22
BC loop	30, 33, 34	31
CC', C'D loops	42sc, 43	46, 47, 48
D strand		53
DE loop	58, 59	
E strand	64, 65, 66, 70	67, 69
F strand	83sc	
FG loop		86, 88
G strand, C-term	91, 93, 97	

This efficiency, in turn, depends on experimental conditions (power missettings, radiofrequency inhomogeneity, specific selective pulse shape) but the issue was no further investigated for the low sample concentrations. A remarkable aspect of the attenuation profile distribution reported in Fig. 6d for D76N β2m is the analogy with respect to the involvements observed for the wild-type species.[4] Both proteins share an interaction interface that includes the N-terminal segment, the B strand, the BC loop and the DE loop. However D76N β2m shows a more extended attenuation surface that requires modelling analysis as performed for wild-type to reach a consistent picture with the experimental NMR evidence.

Modelling D76N β2m interaction with Cit-AuNPs

Based on the previous modelling of wild-type β2m and Cit-AuNPs system,[4] calculations were set up using the same framework for building the charged Au surface and the citrate adsorption layer (ad-layer). The subsequent docking of D76N β2m to the citrate-coated NPs was followed by 20 ns replica exchange molecular dynamics (REMD) calculations at different temperatures (T-REMD) – overall, for 32 replicas, yielding an aggregated simulation time of 640 ns - to enhance energy-barrier crossing and reduce possible drawbacks from local-minimum-energy states.[20,21,4] This protocol reproducing the one employed with wild-type protein,[4] led to results that did not match the experimental pattern from NMR attenuations. In particular the fully-atomistically refined D76N β2m monomer, in addition to the N-terminal, BC and DE loop, exhibited systematic contacts with the NP surface that extensively involved AB loop, during T-REMD. This latter loop, however, showed poor or no involvement at all in the NMR monitored samples, except for the attenuation of Glu16 or His13 NHs observed, respectively, at protein/NP ratio of 107 or 203. The experimental NMR results could then reflect inter-monomer interactions, more pronounced for D76N β2m with respect to wild-type consistently with enhanced amyloidogenicity. The association of wild-type β2m or variants into dimers and, to reduced extents, larger oligomers has been frequently observed experimentally.[22-24] Therefore a preliminary docking to build a D76N β2m dimer was performed, followed by MD refinement and then by 20 ns T-REMD of the interaction of D76N β2m dimer with Cit-AuNPs. Fig. 7a shows the result of the protein-protein docking. The dimer represents the most populated encounter complex of D76N β2m (accounting for 97% of the encounters). The main parameters of docking optimization are reported in Table 3. The interaction surface in the dimer displays contacts between Phe22, Ile46, Glu47, Lys48, Asp53, Tyr67, Glu69 on first protein, and Thr4, Pro5, His31, Thr86 and Ser88 on the second protein, i.e. AB and CD loops, D and E strands on one

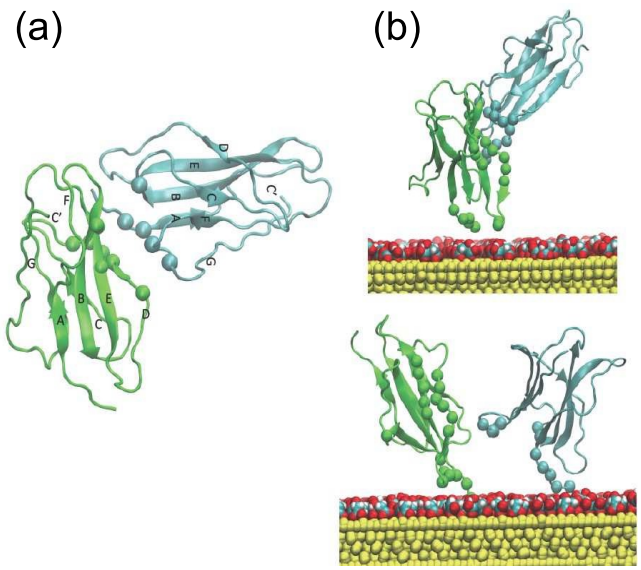

Fig. 7 (a) D76N β2m dimer as obtained from the optimised docking protocol. Direct contacts between the monomers are established between Gln2, His31 and Ser88 of first monomer (green) and Asp53, Thr68 and Glu69 of second monomer (cyan). (b) interaction of D76N β2m dimer with Cit-AuNPs surface leading to separation into monomers. The splitting of the dimer from the starting pose (upper frame) was obtained after 20 ns of T-REMD.

Table 3 Summary of results for the most populated encounter complex of two D76N β2m proteins as obtained by docking.

RelPop %[(a)]	URepr [(b)]	Upds[(c)]	UEP[(d)]	Spread[(e)]
97	-21.821	-15.287	-11.624	1.462

[(a)] Relative population
[(b)] URepr: total interaction energy of the representative structure of the cluster in kT with T= 300 K
[(c)] Upds: non-polar (hydrophobic) desolvation energy of the representative complex, in kT
[(d)] UEP: total electrostatic energy of the representative complex, in kT
[(e)] RMSD of the structures within the cluster with respect to the representative complex in Å.

side and N-terminal, AB and FG loops on the other. When this dimer is submitted to docking to the gold surface and subsequent T-REMD on Cit-AuNPs surface, the final state displays a condition where the dimer has been essentially disassembled (Fig. 7b), with the two monomers interacting with the citrate layer through the N-terminal fragment or the DE loop. The crucial points of this result are the following: i) the significance of an interaction with Cit-AuNPs that essentially brings about dimer detachment, i.e. the disruption of the very first step of aggregation; ii) the matching of the dimer interface region and the attenuation pattern undergone by D76N β2m in presence of Cit-AuNPs (Table 2). Although T-REMD calculations account for the protein approaching the Cit-AuNPs only at the N-terminal stretch and at the DE loop to link directly contacts and attenuations, the similar NMR intensity changes in protein regions that coincide or are adjacent to the dimerization surface suggest some mechanism entailing allosteric perturbation for those attenuation escaping the scheme of direct contacts with NP surface. Considering the protein structure and the data of Table 2, this may be the case for the attenuations involving AB loop, start of B strand, CC' and C-terminal segments (residues 13, 16, 21sc, 42sc, 43 and 97), all the other experimental attenuations being consistently reconciled with adjacent areas to the protein—NP contacts sampled by T-REMD simulations, i.e. N-terminal stretch and DE loop. To investigate this point further, we additionally performed configurational principal component analysis of the two identical protein interacting in solvent, to reveal the structures underlying the atomic fluctuations and the region with the highest degree of correlation, which may be directly connected to protein allostericity. For the three modes with largest correlation scores that were identified, one protein of the dimer shows dominant fluctuations at the AB loop, DE loop and FG loop region in the first collective motion. Similarly, in both the second and third collective modes, fluctuations of the AB loop appear to be correlated to the fluctuation of the opposite DE loop, resembling the allosteric perturbations observed in the NMR experiments (ESI Fig. S2a†). Structural fluctuations are less pronounced in the other monomer (ESI Fig. S2b†).

Effect of Cit-AuNPs on D76N β2m fibrillogenesis

The mild conditions necessary for the fibrillogenesis of D76N β2m (37 °C, neutral pH and agitation) are compatible with the stability of Cit-AuNPs suspensions offering the possibility of investigating their effects on fibrillogenesis in a physiological, although *in vitro*, environment. The fibril formation was analysed through three different methods: thioflavin T (ThT) fluorescence, TEM and native agarose gel electrophoresis. Thioflavin T is a dye whose fluorescence sharply increases upon binding with highly ordered amyloid structures and this fluorescence intensity is proportional to the fibril concentration.[21] The ThT assay (Fig. 8) showed that in presence of Cit-AuNPs the amount of fibres is lower compared to the control sample. To rule out the possibility of fluorescence quenching by the nanoparticles, we compared the ThT fluorescence intensity of D76N β2m mature fibrils in the absence and in the presence of Cit-AuNPs. Since the measured values were the same in both samples, we reasonably inferred that the ThT assay result shown in Fig. 8 reflects a partial inhibition of fibrillogenesis caused by the presence of Cit-AuNPs. The fluorescence intensity values suggest that after 30 hours Cit-AuNPs reduce the amount of fibres by 60%. This result was further confirmed by TEM images in which fibres could hardly be detected when D76N β2m was incubated with Cit-AuNPs, as opposed to the sample incubated without

nanoparticles (Fig. 9). In the attempt to clarify the observed inhibition of D76N β2m fibrillation, a soluble fraction analysis of the protein samples incubated under fibrillogenic conditions,

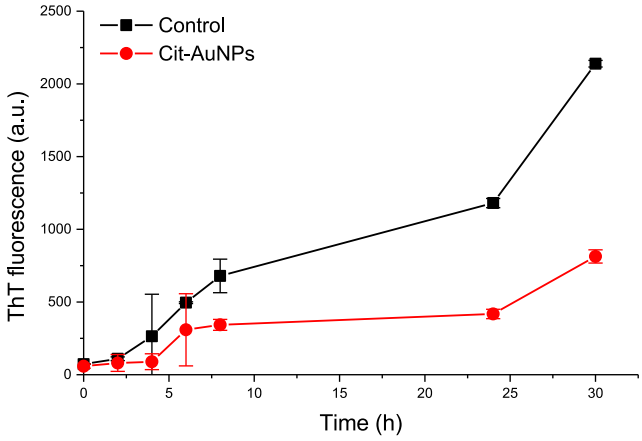

Fig. 8 Fibrillogenesis of 20 μM D76N β2m monitored by means of ThT fluorescence intensity in the control sample (black line) and in the presence of Cit-AuNPs (red line). Measurements were always performed in triplicate.

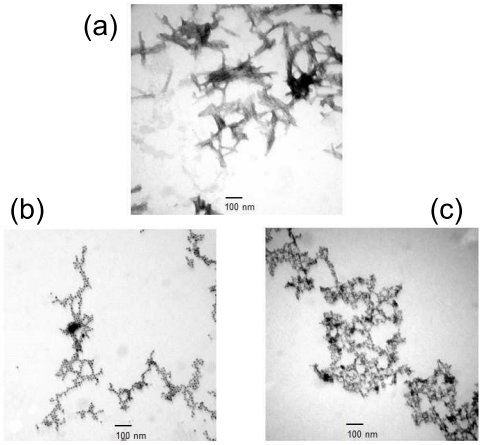

Fig. 9 TEM micrographs of 20 μM D76N β2m incubated under fibrillogenic conditions (a) in the absence of Cit-AuNPs, (b) and (c) in presence of Cit-AuNPs. Fibres are massively present in (a), totally absent in (b) and (c). The aggregate observed in (c) is not fibrillar although it may be ThT positive.

with and without Cit-AuNPs, was undertaken through native agarose gel electrophoresis (Fig. 10). The gel showed a decreased amount of soluble protein from the very beginning in presence of Cit-AuNPs, when no aggregation had yet occurred according to Fig. 8. A fraction of the dissolved protein, indeed, was systematically dragged out with the nanoparticle sediment by the centrifugation step preceding electrophoresis, as confirmed also by UV control of the supernatant. This dragging out was ascertained even under static, i.e. non-fibrillogenic, conditions. Centrifugation of D76N β2m solutions, statically incubated with Cit-AuNPs, led to some 40-50% loss of the initially loaded protein in comparison with the same sample without Cit-AuNPs, as determined from band intensity of native

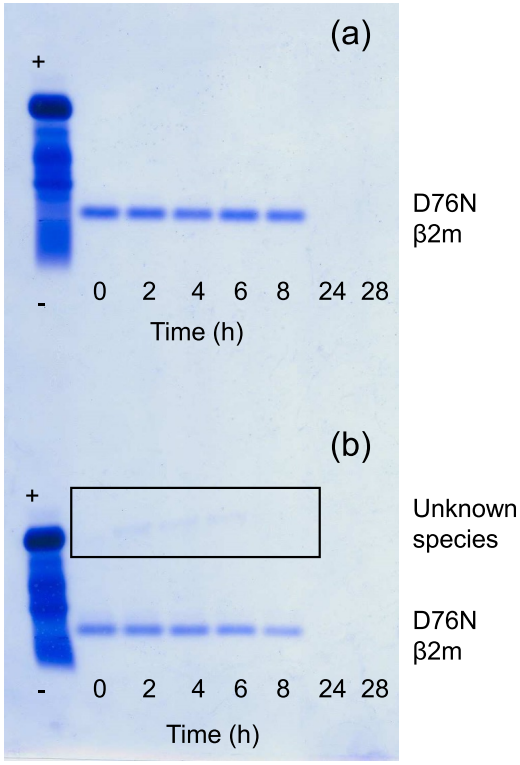

Fig. 10 Native agarose gel electrophoresis of 20 μM D76N β2m exposed to fibrillogenic conditions (a) without Cit-AuNPs and (b) with Cit-AuNPs, at different incubation times. Gels were stained with Coomassie blue. The band corresponding to the second species appearing in the presence of Cit-AuNPs is highlighted by a black box.

agarose gel electrophoresis (ESI Fig. S3†) or UV assay on supernatant.

In fibrillogenic conditions, after 8 hours of incubation, a progressive protein aggregation was estimated by a reduction of band density related to monomeric D76N β2m (Fig. 10). The corresponding kinetics, expressed as complementary precipitation percentage, proved independent of the presence of Cit-AuNPs (Fig. 11). All these finding suggest that the substantial inhibition of D76N β2m fibrillation displayed in Fig. 8 arises genuinely from the presence of Cit-AuNPs that are able to compete with the protein fibrillation pathway. The extent of inhibition is dependent on the protein/NP ratio, as shown in Fig. 12. With a fixed concentration of Cit-AuNPs (25 nM), increasing the protein concentration raises the amount of protein that undergoes fibrillogenesis because of increasing saturation of the interaction sites onto the Cit-AuNPs surface. With simple geometrical considerations,[25] for spherical Cit-AuNPs with average diameter of 7.5 nm, it can be estimated

that some 55-95 D76N β2m monomers can be accommodated around the nanoparticle surface, considering the protein as a cylindroid with longitudinal and transverse axes of 4.3-3.8 and 2.5-2.0 nm, respectively.[26] This volume-based estimate, that appears unrealistic in terms of packing density, would be reduced to 33-49 if the ratio of Cit-AuNP surface area and protein cylindroid base is considered at maximum packing density.[27]

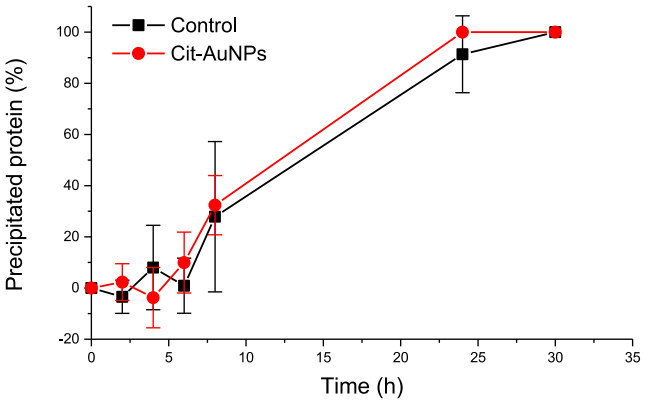

Fig. 11 Precipitation kinetics measured by densitometric analysis of the bands in native agarose gel electrophoresis of the control (black) and the sample incubated with Cit-AuNPs (red). The reported values were normalized by considering the respective band density at Time = 0. The experiment was done in triplicate and the errors are the standard deviations. In spite of conspicuous deviations at early times, the relative precipitation kinetics profiles are essentially superimposable.

Moreover the mentioned saturation effect is consistent with the smoothing observed for the protein signal attenuations observed by NMR on increasing the protein/NP ratio. Native gel electrophoresis showed an additional feature. After two hours of incubation, in presence of Cit-AuNPs another species with different electrophoretic mobility in comparison with the monomer was sampled (Fig. 10b). This species was systematically detected only under fibrillogenic conditions (Fig. S3b†) and in presence of Cit-AuNPs. However, it invariably disappeared in conjunction with the monomeric species. An origin of that band due to electrophoretic migration of Cit-AuNPs can be ruled out considering the Coomassie staining negativity of the nanoparticles (ESI Fig. S4c†). In addition, by increasing the centrifugation time, essentially complete precipitation of Cit-AuNPs was reached as confirmed by UV-Vis, but the low-mobility species was still present (ESI Fig. S5d†). All the evidence then point to an oligomeric/aggregated protein species that accumulates only in the presence of Cit-AuNPs and accompanies a reduced fibrillogenesis pattern. The latter, in fact, while being qualitatively analogous to the control profile, remains quantitatively well below the control levels measured in absence of Cit-AuNPs.

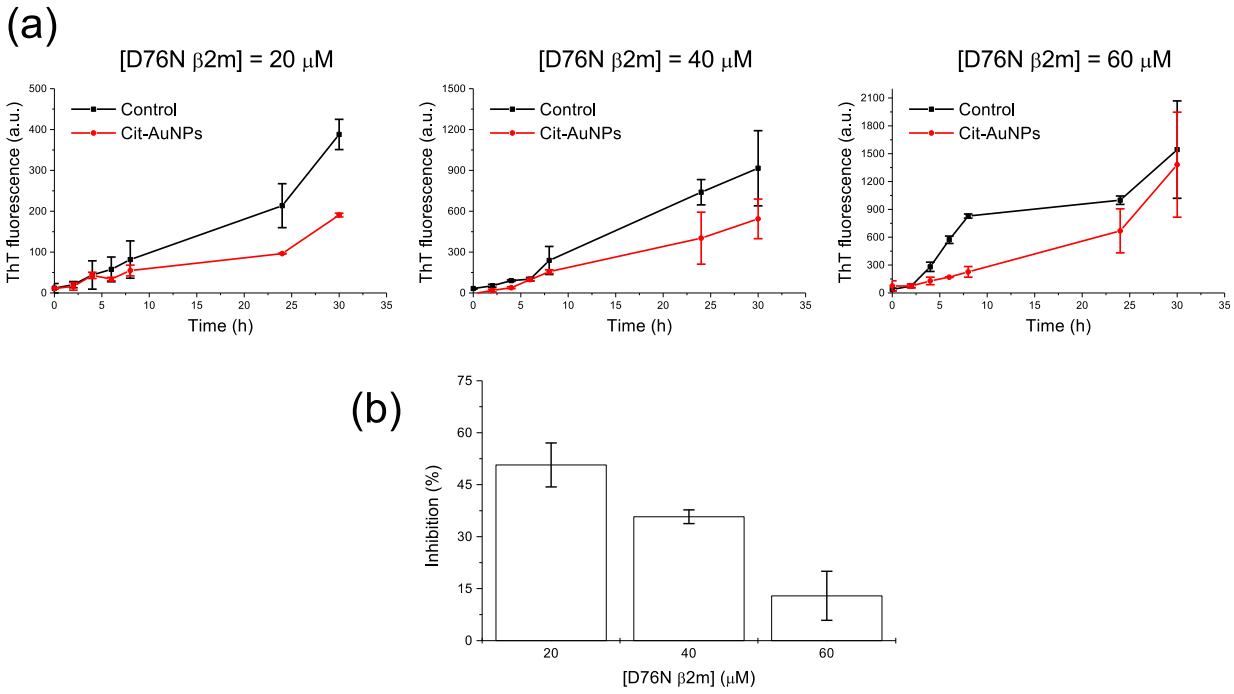

Fig. 12 (a) ThT-based monitoring of D76N β2m fibrillogenesis at varying protein concentrations in absence (black) and in presence of ~ 25 nM Cit-AuNPs (red) and (b) bar plot representing the inhibitory capability of Cit-AuNPs at different protein concentrations measured considering the final ratios of ThT fluorescence values reported in panel a. All measurements were always performed in triplicate and bars represent the corresponding standard deviations. Note that vertical scales differ in panel a.

Conclusions

The characterization of the interaction between Cit-AuNPs and D76N β2m, the naturally occurring highly amyloidogenic variant of β2m, has revealed the dynamic regime of the process. By NMR we have mapped preferential interaction sites on the protein surface that have been properly reproduced by modelling calculations only when a dimeric assembly was considered. The dimer is reshaped and eventually split in the presence of Cit-AuNP surface, and thus also protein interface becomes involved in contacts with that surface. Most significantly, *in vitro* fibrillogenesis shows a substantial reduction when carried out in presence of Cit-AuNPs. These results enable us to conclude that the interaction of D76N β2m with Cit-AuNPs interferes with the early aggregation events of the protein that must occur at the very onset of the amyloidogenic pathway, namely at the level of protofibril formation or recruitment. Ultimately, Cit-AuNPs hamper D76N β2m fibril deposition, opposite to previous results reported in the literature and obtained with other nanoparticles such as polymeric nanoparticles, cerium oxide nanoparticles, quantum dots and carbon nanotubes, that were found to promote β2m fibrillogenesis.[6] Therefore new perspectives can be viewed for nanoparticle applications with amyloidogenic proteins and the burdens still represented by nanoparticle concentration limits and general biocompatibility problems[3] only stimulate further the research challenge in the field.

Experimental section

Materials

All reagents were used as received, without further purification. Tetrachloroauric(III) acid trihydrate, trisodium citrate dihydrate, sodium borohydride, thioflavin T and HEPES were purchased from Sigma-Aldrich. D76N β2m, either unlabeled or ^{15}N-uniformly-labeled and wild-type β2m, only unlabeled, came from overexpression in transformed *E. coli* BL21DE3 strains, according to the procedures previously described.[7,26] Their concentrations were determined spectroscopically by recording absorbance at 280 nm using a molar extinction coefficient of 19,940 M^{-1} cm^{-1} calculated from the primary sequence using the ExPASY online tool.[28] Unless otherwise specified, the lyophilized proteins were dissolved in 50 mM HEPES buffer at pH 7. Thioflavin T concentration was determined spectroscopically, measuring the absorbance at 412 nm using an extinction coefficient of 36,000 M^{-1} cm^{-1}.[29]

Cit-AuNPs synthesis and characterization

Only for NMR measurements, citrate-stabilized AuNPs were obtained from Sigma-Aldrich, as 90 nM suspension with nanoparticle average diameter of 5 nm. For any other purpose we used Cit-AuNPs from our synthesis because more convenient for reproducibility checks in terms of size, coating, impurity content, etc. When tested with wild-type β2m, the in-house preparations were reproducibly shown to give the same NMR results as the Sigma product. Besides the convenience of homogeneous comparison, the commercial product was preferred for NMR measurements on D76N β2m because of the higher concentration with respect to the in-house synthesized product. At the selected protein/AuNP ratios, in fact, higher protein concentrations could be employed to improve sensitivity and measurement time. All glassware used in nanoparticle synthesis was washed with *aqua regia* and dried in hoven before use. To prepare citrate stabilized gold nanoparticles with a size range from 5 to 10 nm, a standard cold synthesis using $NaBH_4$ as gold reducing agent was employed,[25] varying the gold/citrate ratio. A solution of sodium citrate dihydrate (1.5 mM) and $HAuCl_4$ trihydrate (0.5 mM) in milliQ water was reduced under stirring at 0 °C by 1 mL of freshly prepared ice-cold $NaBH_4$ solution (0.1 M). The reduction of Au(III) to Au(0) and the consequent formation of the nanoparticles stabilized by the presence of citrate was assessed by the instantaneous colour change of the solution from pale yellow to ruby red after the addition of the reductant. The solution was allowed to reach room temperature under stirring and then was stored at 4 °C. The Cit-AuNPs were fully characterized by UV-Vis spectroscopy and transmission electron microscopy (TEM). The concentration of reduced gold (Au^0) was determined by the UV-Vis absorbance of the colloidal solution at 400 nm[30] and used to estimate the molar concentration of nanoparticles considering the average number of gold atoms per nanoparticle (*N*) expressed by the following equation:[31]

$$N = \frac{\pi \rho d^3}{6\,M} = 30.89602 d^3$$

where d is the nanoparticles diameter, ρ is the density for fcc gold (19.3 g/cm^3) and M stands for atomic weight of gold (197 g/mol). The analysis of the nanoparticle surface plasmon resonance (SPR) in the UV-Vis spectrum in absence and in presence of 20 μM D76N β2m was performed with a JASCO UV-530 spectrophotometer by acquiring a spectrum in the range from 400 to 600 nm with a band-width of 2.0 nm, a data pitch of 0.2 nm and a speed of 40 nm/min. TEM images were recorded using a Tecnai G2. 5 μL of Cit-AuNP solution were dropped on a Cu 400-mesh TEM grid and left at room temperature for 3 hours to allow for solvent evaporation. The size distribution was calculated by measuring a minimum of 200 particles using the ImageJ software.[32]

NMR spectroscopy

NMR samples were prepared by dissolving liophylized ^{15}N-labeled D76N β2m in 25 mM phosphate buffer to obtain 1 mL mother solution, at approximately 0.3 mM protein concentration. Suitable aliquots (10, 15, 20 µL, etc.) were diluted to 0.5 mL with the previous buffer, lyophilized and redissolved in either 0.5 mL H_2O/D_2O 93/7 with 1.3 mM trisodium citrate or in the Sigma-Aldrich 90 nM Cit-AuNPs suspension with the addition of 7% D_2O. In this way pairs of 4.5, 8.9 and 18 µM protein solutions, with and without Cit-AuNPs, were obtained at pH* 6.8 (pH* = uncorrected pHmeter reading). NMR spectra were collected at 14.0 T, on the Bruker Avance III NMR facility of the Core Technology Platform at New York University Abu Dhabi. The spectrometer, equipped with cryoprobe and *z*-axis gradient unit, operated at 600.13 and 60.85 MHz to observe ^{1}H and ^{15}N, respectively. In addition to 1D control spectra, 2D ^{15}N-^{1}H HSQC[33] were recorded over spectral widths of 40 ppm (^{15}N, t_1) and 15 ppm (^{1}H, t_2), and digitized over 128 and 2048 points, respectively. For each t_1 dimension point, 128 or 64 scans were accumulated and quadrature in the same dimension was accomplished by gradient-assisted coherence selection (echo-antiecho).[34] Processing with t_1 linear prediction, apodization and zero-filling prior to Fourier transformation led to 2K×1K real spectra. Water suppression was achieved by using a flip-back pulse in the HSQC experiments.[19] All measurements were performed at 25 °C.

Fluorescence quenching

Wild-type and D76N β2m intrinsic fluorescence was recorded in absence of Cit-AuNPs and after the progressive addition of small amounts of nanoparticles using a Perkin Elmer LS-55 fluorimeter. For the measurement, fluorescence semi-micro cuvettes were used (5 mm x 5 mm). The samples were excited at 295 nm and the emission was recorded from 300 to 450 nm, using 5 nm slit for both excitation and emission. Each spectrum was the average of 5 consecutive measurements and the quenching efficiency parameters are reported as an average of three individual experiments, along with the standard deviation, for each protein. The protein concentration was kept constant at 0.5 µM and the nanoparticle concentration ranged from 0 to 0.8 nM. The measured fluorescence intensity (F_{meas}) was corrected for the inner filter effect using the following equation:[15]

$$F_{corr}=F_{meas}\ 10^{(A_{ex}+A_{em})/2}$$

where A_{ex} and A_{em} are the Cit-AuNPs absorbances at excitation and emission frequencies, respectively.

To compare qualitatively the quenching efficiency of low Cit-AuNPs concentrations on the wild-type and D76N β2m, the fluorescence data can be fitted with the linear Stern-Volmer equation:[15]

$$\frac{F_0}{F}=1+K_{SV}[NP]=1+k_q\tau_0[NP]$$

where F_0 and F are the fluorescence intensities of the protein in absence and in presence of Cit-AuNPs, respectively and the Stern-Volmer constant, K_{SV}, is the product of the diffusion-limited bimolecular quenching constant, k_q, and the fluorophore fluorescence lifetime, τ_0.

To estimate the order of magnitude of the binding constants, the Hill equation was applied.[16] The fluorescence quenching was expressed by the following relation:

$$Q=\frac{F_0-F}{F_0}$$

The saturation value of Q is:

$$Q_{max}=\frac{F_0-F_\infty}{F_0}$$

Since AuNPs are able to quench completely the protein fluorescence, F_∞ can be set to 0 and consequently $Q_{max}=1$.[16] Following Lacerda et al.,[16] Hill equation can be written as:

$$\frac{Q}{Q_{max}}=\frac{[L]^n}{(K_d+[L]^n)}$$

where L stands for Cit-AuNPs, K_d represents the apparent dissociation constant and n is the Hill coefficient, in this context related the cooperativity of the binding.

The standard error connected to the fit is expressed as $\sigma_i = (C_{ii}\ \chi^2)^{1/2}$ where C_{ii} is the diagonal element of the variance-covariance matrix and χ is the standard statistical correlation index.

Modeling

Rigid-body docking simulations were carried out using Brownian dynamics (BD) techniques with the ProMetCS continuum solvent model for protein_gold surface interactions.[35] Protocols were similar to the ones adopted for wild-type protein and previously described in detail, [4] therefore will not be repeated here. The calculations were performed using the SDA version 7.2 software.[36] The Au(111) surface was constructed with a surface area of 100 Å × 100 Å and three atomic layers.[37] The D76N β2m structure was obtained by introducing the asparagine substitution for the aspartate at position 76 in the NMR solution structure of β2m[26] (PDB code 1JNJ). Protein-protein docking is used to obtain the most stable D76N-D76N encounter complexes which are then refined by T-REMD both in solvent and on Cit-AuNPs with solvent.

D76N β2m fibril formation

A solution of D76N β2m (2 mg/mL) in 50 mM HEPES pH 7 was centrifuged (14,000 rpm, 10 minutes). The supernatant was collected as much as possible without the pellet and filtered with a filter of 0.22 µm. After the concentration measurement, the solution was diluted to 20 µM either with buffer containing 1.5 mM sodium citrate or with Cit-AuNPs buffered suspension resulting in 25 nM constant NP concentration. Sodium azide (1‰) was added as preservative. The solutions were incubated at 37 °C under vigorous stirring. Aliquots were taken at

different time points to perform fibrillation analysis. The experiments were done in triplicate.

Thioflavin T assay

A 10 μM ThT solution in 50 mM glycine buffer at pH 8.3 was prepared. This solution was added to the samples collected during the fibrillation and fluorescence was recorded at 480 nm, after excitation at 445 nm on a Perkin Elmer EnSpire 2300 fluorimeter.

Trasmission electron microscopy imaging of fibrils

Some drops of the solutions incubated under fibrillogenic conditions were deposited on a TEM grid and after 5 minutes the excess was soaked up with filter paper. The preparations were stained with some drops of 2% uranyl acetate solution in water for 5 minutes, the remaining solution was removed with filter paper and the grid was washed with water and dried for 10 minutes. The samples were observed using the transmission electron microscope Philips EM 208 at the Electron Microscopy Centre of the University of Trieste for the characterization of Cit-AuNPs with and without D76N β2m or Joel 1200EX at the EM Unit of the UCL Division of Medicine in London, UK for the samples after fibrillogenesis.

Native agarose gel electrophoresis

An aliquot of 10 μL of D76N β2m solution incubated under fibrillogenic conditions was centrifuged at 14,000 rpm for 10 minutes. The supernatant was collected and frozen. The samples were loaded onto 1% agarose gel and the protein was stained with Coomassie Blue. The analysis of the gel were performed using ImageJ software. [32]

Acknowledgements

The work received financial support from PRIN project No. 2012A7LMS3.

We acknowledge the New York University Abu Dhabi for access to the Core Technology Platform. We also thank Alejandra Carbajal and the Division of Medicine Electron Microscopy Unit, Royal Free Campus, University College London for the amyloid fibril images.

Notes and references

1 I. Lynch and K. A. Dawson, *Nano Today*, **2008**, *3*, 40–47.
2 S. R. Saptarshi, A. Dusch and A. L. Lopata, *J. Nanobiotechnology*, **2013**, *11*, 26-37.
3 P. Wang, X. Wang, L. Wang, X. Hou, W. Liu and C. Chen, *Sci. Technol. Adv. Mater.*, **2015**, *16*, 1-15.
4 G. Brancolini, A. Corazza, M. Vuano, F. Fogolari, M. C. Mimmi, V. Bellotti, M. Stoppini, S. Corni and G. Esposito, *ACS Nano,* **2015**, *9*, 2600-2613.
5 F. Gejyo, T. Yamada, S. Odani, Y. Nakagawa, M. Arakawa, T. Kunitomo, H. Kataoka, M. Suzuki, Y. Hirasawa, T. Shirahama, *et al., Biochem. Biophys. Res. Commun.,* **1985**, *129*, 701–706.
6 S. Linse, C. Cabaleiro-Lago, W.-F. Xue, I. Lynch, S. Lindman, E. Thulin, S. E. Radford and K. A. Dawson, *Proc. Natl. Acad. Sci.,* **2007**, *104*, 8691-8696.
7 S. Valleix, J. D. Gillmore, F. Bridoux, P. P. Mangione, A. Dogan, B. Nedelec, M. Boimard, G. Touchard, J.—M. Goujon, C. Lacombe, P. Lozeron, D. Adams, C. Lacroix, T. Maisonobe, V. Planté-Bordeneuve, J. A. Vrana, J. D. Theis, S. Giorgetti, R. Porcari, S. Ricagno, *et al., Engl. J. Med.,* **2012**, *366*, 2276-2283.
8 P. P. Mangione, G. Esposito, A. Relini, S. Raimondi, R. Porcari, S. Giorgetti, A. Corazza, F. Fogolari, A. Penco, Y. Goto, Y.-H. Lee, H. Yagi, C. Cecconi, M. M. Naqvi, J. D. Gillmore, P. N. Hawkins, F. Chiti, R. Rolandi, G. W. Taylor, M. B. Pepys *et al., J. Biol. Chem.,* **2013**, *288*, 30917-30930.
9 G. Mie, *Ann. Phys.,* **1908**, *25*, 377-445.
10 P. V. Kamat, *Phys. Chem. B,* **2002**, *106*, 7729-7744.
11 W. P. Hall, S. N. Ngatia and R. P. Van Duyne, *J. Phys. Chem. C,* **2011**, *115*, 1410-1414.
12 P. Joshi, V. Shewale and R. J. Pandey, *Phys. Chem. C,* **2011**, *115*, 22818-22826.
13 M. Kihara, E. Chatani, K. Iwata, K. Yamamoto, T. Matsuura, A. Nakagawa, H. Naiki and Y. Goto, *J. Biol. Chem.,* **2006**, *281*, 31061-31069.
14 J. R. Lackowicz, *Principles of fluorescence spectroscopy*, second edition, ed. Plenum Press, New York, 1999.
15 H. D. P. Lacerda, J. J. Park, C. Meuse, D. Pristinski, M. L. Becker, A. Karim and J. F. Douglas, *ACS Nano,* **2010**, *4*, 365-379.
16 J. Gao, Y. Lai, C. Wt and Y. Zhao, *Nanoscale,* **2013**, *5*, 8242-8248.
17 M. van de Weert and L. Stella, *J. Mol. Struct.,* **2011**, *998*, 144-150.
18 E. Dulkeith, A. Morteani, T. Niedereichholz, T. Klar, J. Feldmann, S. Levi, F. van Veggel, D. Reinhoudt, M. Möller and D. Gittins, *Phys. Rev. Lett.,* **2002**, *89*, 203002.
19 S. Grzesiek and A. Bax, *J. Am, Chem. Soc.,* **1993**, *115*, 12593-12594.
20 Y. Sugita and Y. Okamoto, *Chem. Phys. Lett.,* **1999**, *314*, 141–151.
21 U. H. E. Hansmann, *Chem. Phys. Lett.,* **1997**, *281*, 140–150.
22 S. Giorgetti, S. Raimondi, K. Pagano, A. Relini, M. Bucciantini, A. Corazza, F. Fogolari, L. Codutti, M. Salmona, P. Mangione, L. Colombo, A. De Luigi, R. Porcari, A. Gliozzi, M. Stefani, G. Esposito, V. Bellotti and M. Stoppini, *J. Biol. Chem.*, **2011**, *286*, 2121-2131.
23 D. Gümral, F. Fogolari, A. Corazza, P. Viglino, S. Giorgetti, M. Stoppini, V. Bellotti and G. Esposito, *Magn. Res. Chem.*, **2013**, *51*, 795-807.
24 G. Esposito, M. Garvey, V. Alverdi, F. Pettirossi, A. Corazza, F. Fogolari, M. Polano, P. P. Mangione, S. Giorgetti, M. Stoppini, A. Rekas, V. Bellotti, A. J. Heck and J. A. Carver, *J. Biol. Chem.*, **2013**, *288*, 17844-17858.
25 L. Calzolai, F. Franchini, D. Gilliland and F. Rossi, *Nano Lett.,* **2010**, *10*, 3101-3105.
26 G. Verdone, A. Corazza, P. Viglino, F. Pettirossi, S. Giorgetti, P. Mangione, A. Andreola, M. Stoppini, V. Bellotti and G. Esposito, *Protein Sci.*, **2002**, *11*, 487-499.
27 Y. Teshima and T. Ogawa, *Forma*, **2000**, *15*, 347-364.
28 https://www.expasy.org/ .
29 M. Groenning, *J. Chem. Biol.,* **2010**, *3*, 1-18.
30 T. Hendel, M. Wuithschick, F. Kettemann, A. Birnbaum, K. Rademann and J. Polte, *J. Anal. Chem.,* **2014**, *86*, 11115-11124.
31 X. Liu, M. Atwater, J. Wang and Q. Huo, *Colloid Surface B,* **2007**, *58*, 3.
32 W. S. Rasband, ImageJ, U. S. National Institutes of Health, Bethesda, Maryland, USA, http://imagej.nih.gov/ij/, 1997-2016.
33 G. Bodenhausen and D. J. Ruben, *Chem. Phys. Lett.,* **1980**, *69*, 185–189.
34 J. Keeler, R. T. Clowes, A. L. Davis and E. D. Laue, *Methods Enzymol.,* **1994**, *239*, 145–207.

35 D. B. Kokh, S. Corni, P. J. Winn, M. Hoefling, K. E. Gottschalk and R. C. Wade, *J. Chem. Theory Comput.,* **2010**, *6*, 1753–1768.
36 R. R. Gabdoulline and R. C Wade, *Biophys. J.,* **1997**, *72*, 1917–1929.
37 F. Iori, R. Di Felice, E. Molinari and S. Corni, *J. Comput. Chem*., **2009**, *30*, 1465–1476.

